IC-PROCESSED MICRO-MOTORS: DESIGN, TECHNOLOGY, and TESTING

Yu-Chong Tai, Long-Sheng Fan, and Richard S. Muller
Berkeley Sensor and Actuator Center
An NSF/Industry/University Cooperative Research Center
Dep't of EECS and the Electronics Research Laboratory
University of California, Berkeley CA 94720

ABSTRACT

Micro-motors having rotors with diameters between 60 and 120 μm have been fabricated and driven electrostatically to continuous rotation. These motors were built using processes derived from *IC* micro-circuit fabrication techniques. Initial tests on the motors show that friction plays a dominant role in their dynamic behavior. Observed rotational speeds have thus far been limited to several hundred rpm which is a small fraction of what should be achievable if only natural frequency were to limit the response. Experimental starting voltages are at least an order-of-magnitude larger than had been expected (60 volts at minimum and above 100 V for some structures). Observations of asynchronous as well as synchronous rotation between the driving fields and the rotors can be explained in terms of the torque/rotor-angle characteristics for the motors.

I. INTRODUCTION

Design considerations for micro-motors have been discussed recently [1,2]. Successful implementation of both stepping and synchronous motors and initial testing results were presented by our group at the 1988 Int. Electron Devices Meeting [3]. In this paper, we describe new aspects of these motors, including theoretical design, advanced polysilicon technology, and phenomenological mechanisms in several micromotors that have been produced using *IC* processing [4].

II. DESIGN

Shown in Fig. 1 is an SEM photograph of a three-phase micro-motor with 12 stators and a 4-pole rotor that was fabricated using a three-layer-polysilicon process. The radius of the rotor is 60 μm and the air gap between the rotor and stator is 2 μm. Fig. 2 shows a schematic cross section of the motor.

Several design features can be seen from Fig. 2. First, the micro-motor is built on a composite layer composed of 300 nm of silicon dioxide and 1 μm of silicon nitride. This layer helps to prevent electrical breakdown between the motor and the silicon substrate. The 1-μm nitride layer is also needed to protect the oxide from HF etching while the sacrificial layer is being dissolved. Experimentally, we have found that this layer can withstand more than 500 V before breakdown occurs. A second feature is a ground plane, formed of first-layer polysilicon, situated beneath both the rotor and the stator. The ground plane, which acts as an electrostatic shield between the rotor and the substrate, improves the performance of the motor by eliminating vertical Coulombic forces on the rotor which result in increased frictional drag. Another advantage of the ground plane is that it provides the possibility of biasing the rotor since it is in electrical contact with the rotor through its hub. This provides an extra freedom for control of the motor compared to a floating rotor design-- a freedom that might be useful to increase the electrical drive on start-up, for example. Another effective friction-reducing feature in the motor shown in Fig. 2 is the use of silicon-nitride spacers at the vertical walls of the rotor and the stators. Figure 3 magnifies the hub and stator parts to illustrate this feature. The nitride spacer between the rotor and the hub forms a lubricating as well as a wear-protecting material with a smaller coefficient of friction and better wear-withstanding characteristics than are found for polysilicon.

III. FABRICATION

The fabrication process is based on the pin-joint technology, reported in [5,6]. In this discussion, we emphasize techniques to fabricate the design features discussed in the last section. Figure 4 shows the major steps in the motor fabrication. In Fig. 4a formation of the 300-nm thick ground plane on top of the oxide-nitride composite layer is indicated. After this layer is deposited, the wafers are covered with 2.2 μm of phosphosilicate glass(PSG) which acts as the sacrificial layer. After opening anchor spots for the stator, a 1.5 μm second-layer polysilicon is deposited and oxidized to have a 100 nm thermal

TH0249-3|89|0000|0001$1.00©1989 IEEE

oxide on top as shown in Fig. 4b. The polysilicon-oxide composite layer then is plasma-etched to form the rotor and stators. A 340-nm LPCVD nitride is then deposited (Fig. 4c) and reactive-ion-etched(RIE) to form the nitride spacers(Fig. 4 d). The thin oxide layer on the polysilicon is used to protect the polysilicon during the nitride RIE etch. Once the nitride spacers are formed, the process follows the outline already reported [5,6], to form the axle-bushing hub. The completed motor (prior to being freed from the sacrificial support layer) is shown in Fig. 4e.

IV. EXPERIMENTAL PROCEDURE

The setup used to drive the motors is shown in Fig. 5. Its function is as follows: a square-wave, extracted from a pulse generator, is sent to a TTL counter which is linked to a TTL decoder. The decoder sends the three-phase signals to the a high-voltage driver and also feeds back a signal to restart the counter after each three counts.

Three voltage phases are therefore repeatedly generated at the driver circuit and sent through current-limiting resistors to the micro-motors. The frequency of the phase voltage is controlled by the square-wave generator and the magnitude of the phase voltage is controlled by the voltage supplied to the driver.

The voltage phases supplied to the micro-motors are shown in Fig. 6. The twelve stator poles are energized in a three-phase pattern. During tests, the phase voltage is first set to a constant value and the phase frequency then is varied from high to low until rotational motion of the motor is observed (through a video attachment on the microscope). Motor movements are video-recorded to determine the speed of rotation and other dynamical properties.

V. MOTOR DYNAMICS

Two-dimensional numerical simulators are used to determine the static-torque/rotor-position characteristics. The simulation results of the torque/position characteristics associated with 4 equi-positioned stators energized at 100 V (and the remaining 8 grounded) is shown in Fig. 7. The torque on the rotor is obtained by multiplying the simulated torque density times the thickness of the rotor which neglects any three-dimensional effects. Figure 7 has a span of only 90 degrees because the torque/position characteristic is periodic for this 4-pole rotor.

A natural frequency f_N, which arises from energy exchange between the electric field and the moving rotor, is an important motor parameter. The frequency f_N can be calculated by considering the rotor mechanics near an equilibrium ($T = 0$) point and assuming zero friction. Then

$$f_N = \frac{1}{2\pi}\sqrt{\frac{T'}{I}} \tag{1}$$

where I is the rotational inertia of the rotor and $-T'$ is the slope of the T vs. θ curve at $T = 0$.

For the motor of Fig. 1, the rotational inertia of the rotor is 2.01×10^{-20} kg-m^2 and T' is approximated as 1.83×10^{-11} Nt-m/rad. Hence f_N = 1.5 kHz (excitation voltage = 100 V). Note that the T vs. θ curve is roughly linear only between $\pm$ 15°.

When the starting angle θ_s is outside the $\pm$ 15° range, the oscillating frequency will differ from f_N because $T(\theta)$ depends on θ. In general, the oscillating frequency can be calculated from

$$f(\theta_s) = \frac{1}{4\int_0^{\theta_s} \frac{d\theta}{\sqrt{2I^{-1}\int_{\theta_s}^{\theta} T(\eta)d\eta}}} \tag{2}$$

here η is a dummy variable and $T(\eta)$ is the torque in Fig. 7. It is straightforward to show that $f(\theta_s)$ in Eq. (2) reduces to f_N in Eq. (1) inside the $\pm$ 15° range where $T(\theta) \approx -T' \times \theta$. Equation (2) shows that the oscillating frequency is a function of the starting angle θ_s. As seen in Fig. 7, $|T' \times \theta| \geq |T(\theta)|$ for all θ in $[0, \theta_s]$. Hence,

$$f_N = \frac{1}{4\int_0^{\theta_s} \frac{d\theta}{\sqrt{2I^{-1}\int_{\theta}^{\theta_s} T'\eta d\eta}}} \geq \frac{1}{4\int_0^{\theta_s} \frac{d\theta}{\sqrt{2I^{-1}\int_{\theta_s}^{\theta} T(\eta)d\eta}}} = f(\theta_s) \tag{3}$$

Equation (3) shows that f_N (in our case 1.5 kHz for 100 V applied to a single phase of 4 stators) is the maximum oscillating frequency.

Since the electrostatic torque acting on the rotor is proportional to the square of the voltage, the natural frequency at a different phase voltage V_p is

$$f_N(V_p) = 1.5\left(\frac{V_p}{100}\right)^2 \text{ kHz} \tag{4}$$

As an example, if V_p equals 200 V, f_N is 6.1 kHz.

The natural frequency of the motor sets an upper bound for the rate at which the the rotor can respond to a switched field on the stators. We can argue, for example, that $\frac{1}{4f_N}$ is the minimum time for the rotor to travel from a starting angle θ_s to θ = 0 if the initial angular velocity is zero as is the case for start/stop-mode stepping motors. In terms of a maximum rotational speed ω_{max}, we have

$$\omega_{max} = \frac{1}{\frac{1}{4f_N}\times n} \times 60 = \frac{240 f_N}{n} \text{ rpm} \tag{5}$$

where n is the number of steps per revolution. As an example, with V_p = 200 V and n = 12, the maximum speed of our stepping motor is predicted to be 120 krpm using Eq. (5).

Neglected in the analysis presented thus far are loading effects (other than inertia) on the rotor. These effects, principally friction, reduce the effective maximum frequency below the calculations in Eqs. (4) and (5). From our measurements, the frictional effects are completely dominant because the observed maximum rotational speed at 200 V is 150 rpm. With friction, the term $T(\eta)$ in Eq. (2) should be replaced by $T_{net}(\eta)$, the net torque on the rotor which is smaller than $T(\eta)$. At this point insufficient information is available about the frictional mechanisms in our motors to go further with this analysis.

The foregoing discussion refers to open-loop drive of the motors, which is the mode used for our experiments. The natural frequency limitation on rpm could be exceeded with closed-loop control, which would be possible with the addition of a rotor-position sensor.

VI. SYNCHRONOUS AND ASYNCHRONOUS MOTION

Another surprising result from dynamical studies of the motors in addition to the frictional effects discussed above is the observation of asynchronous as well as synchronous motion in the motors. Specifically, we observe that it is possible for the rotor to rotate in opposition to the rotational sense of the phasing field. This behavior, we believe, can be understood in terms of the dynamic balance between electrostatic-drive torque and that due to friction. It is easiest to introduce this concept by considering the motor driven by only one phase of the three-phase voltage drive.

Figure 8 (a) shows the voltage connections for single-phase drive of the motor of Fig. 1 as well as a defining condition for the initial position of the rotor (θ = 30 °). The angle θ in Fig. 8 (a) is measured from a rest (T = 0) position. Shown in Fig. 8 (b) (which is similar to Fig. 7) is the corresponding normalized torque/position characteristic. Indicated by straight lines on Fig. 8 (b) are assumed constant frictional-torque values which, of course, oppose the applied torque T.

Consider that the horizontal stator (in Fig. 8 (a)) is energized. Since T exceeds the frictional value, the rotor will begin to rotate in the clockwise direction and will accelerate until it reaches angle P at which the frictional torque equals the the driving torque. As θ decreases toward zero, the rotor will decelerate due to friction. Whether the rotor passes through θ = 0 depends upon specific values for frictional and driving torque as well as on the rotor inertia. If it passes θ = 0, it will continue to decelerate between θ = 0 and θ = Q. The rotor may stop anywhere between angles P and Q, but if it can pass point Q, it will decelerate more strongly because the driving torque is reversed in this region. If the rotor stops between θ = Q and θ = -30°, it will accelerate again, but this time in a counter-clockwise direction. Once again, the rotor will repeat a similar acceleration-deceleration-stop cycle except that the direction of rotation is different. Several cycles may occur, but eventually the rotor will stop between θ = P and θ = Q.

The final resting place of the rotor after the cyclic motion discussed above (when the motor is energized by a single phase) indicates whether synchronous or asynchronous rotation will occur in the motor when it is driven by three phases.

a) Three-phase synchronous mode

Normalized three-phase torque/position characteristics of the motor are shown in Fig. 9. In Fig. 9, the drive voltages are phased ±30° apart because the motor has twelve stator poles. The starting position is again assumed at θ = 0. In Fig. 9, θ = P and θ = Q are the angles at which frictional and driving torque are in balance for phase A and θ = R is one of the corresponding angles for phase B. We conclude that if a static three-phase excitation of the stator field results in a final resting position for the rotor between θ = P and θ = R or any of the corresponding $\pm\frac{m\pi}{6}$-shifted regions, the motor will operate synchronously (where m is an integer).

The explanation is in the following. Based on the discussion for single-phase excitation above, the rotor would tend to come to rest inside the frictional band, either between θ = P and θ = R, or between θ = R and θ = Q. If the former, then the rotor will rotate counter-clockwise because of the positive, larger-than-friction, driving torque from phase B. A similar behavior would be repeated with respect to phase C so that the rotor would rotate synchronously with the field following phases ...ABCABCABC....

b) Three-phase asynchronous mode

The motor and field rotation will be in opposite directions, however, if the rotor rest position under the conditions described (in section *(a)* above) occurs between θ = R and θ = Q. or its $\pm\frac{m\pi}{6}$-shifted regions. The reason is as follows. If, after phase A, the rotor rests between θ = R and θ = Q, the next phase (B) will not be able to rotate the rotor because inside that region the driving torque produced by this phase is smaller than the maximum frictional torque. However, phase C will apply a negative torque, which can overcome the friction on the rotor and make it rotate in a clockwise direction, opposite to the rotation of the stator fields. For continuous motion phase C must leave the rotor at rest between θ = R" and θ = Q". Then, next phase A will not be able to turn the rotor because of the friction. However, the next cycle of phase B will again cause clockwise rotation. A feature of this motion is that the rotor rotates at only one-half the frequency of the driving

fields because it is driven only during a half cycle of one phase; for an applied signal ...ABCABC..., the rotor rotates ...ACBACB....

Experimentally, both modes have been observed. In some cases, it appears that both synchronous and asynchronous behavior alternates spontaneously. It is believed this behavior can be explained by irregular friction in real motors, since friction determines the critical angle values for the rotational variations described above.

VII. CONCLUSIONS

Initial tests of electrostatically-driven *IC*-processed micromotors show that frictional effects play a dominant role in their dynamic behavior. Rotational speeds in these motors are only a small fraction of what should be achievable if only natural frequency were to limit the response of the rotor. The experimental starting voltages are at least an order-of-magnitude larger than had been expected (60 volts at minium and above 100 V for some structures).

Observations of asynchronous as well as synchronous rotation between the driving fields and the rotors are explained in terms of the torque/rotor-angle characteristics.

Acknowledgements We thank Profs. D.J. Angelakos, R.M. White, D. Giandomenico, and Paul T. Yang for valuable discussion, and K. Voros, R. Hamilton, and the staff of the Berkeley Microfabrication Laboratory for assistance in processing.

REFERENCES

[1] W.S. Trimmer and K.J. Gabriel, "Design Considerations for a Practical Electrostatic Micromotor," *Sensors and Actuators*, 11, 189-206, (March, 1987).

[2] S.F. Bart, T.A. Lober, R.T. Howe, J. H. Lang, and M.F. Schlecht, "Design Considerations for Microfabricated Electric Actuators," *Sensors and Actuators*, 14, 269-292 (July, 1988).

[3] L.S. Fan, Y.C. Tai, and R.S. Muller,"IC-processed Electrostatic Micro-motors," *1988 IEEE Int. Electr. Devices Meeting*, 666-669, San Francisco, CA, December 11-14, 1988.

[4] *Patent Pending*.

[5] R.S. Muller, L.S. Fan, and Y.C. Tai, "Micromechanical Elements and Methods for Their Fabrication," U.S. Patent 4,740,410, issued to the Regents of the University of California, April 26, 1988.

[6] L.S. Fan, Y.C. Tai, and R.S. Muller,"Integrated movable micromechanical structures for sensors and actuators," *IEEE Trans. Electro. Devices*, vol. **ED-35,** pp.724-730, June 1988.

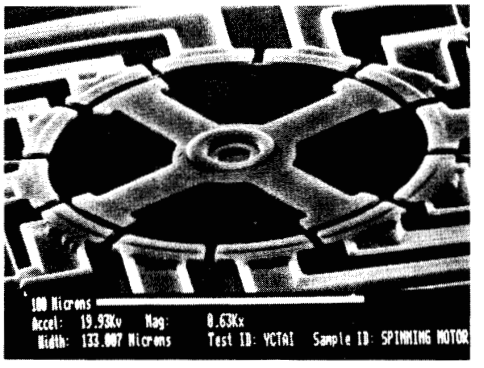

Figure 1. SEM photograph of a fabricated micromotor; rotor diameter = 120 μm.

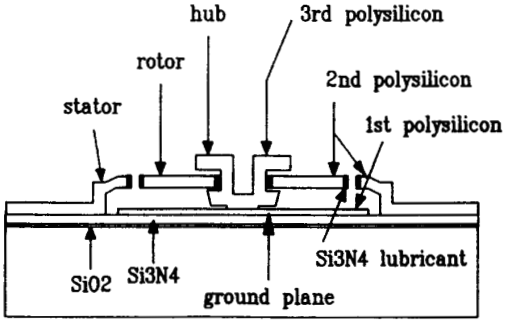

Figure 2. Schematic cross section of the micro-motor in Fig. 1.

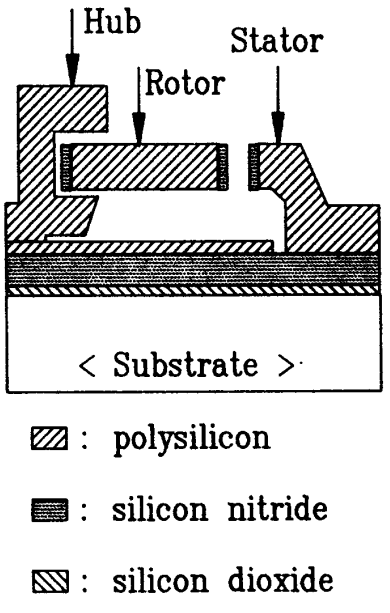

Figure 3. Cross section showing construction of the hub, rotor, and stator for the micro-motor of Fig. 1.

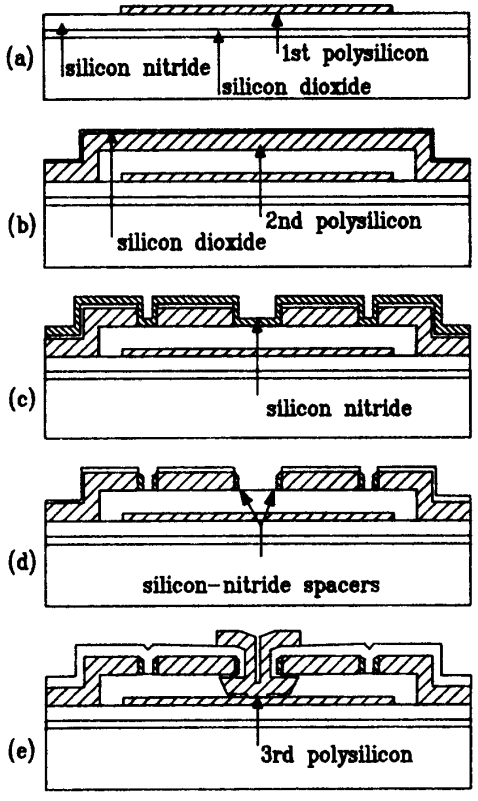

Figure 4. Major fabrication steps to construct the micro-motors.

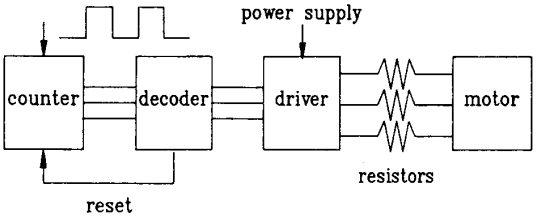

Figure 5. Setup for 3-phase drive of the micro-motors.

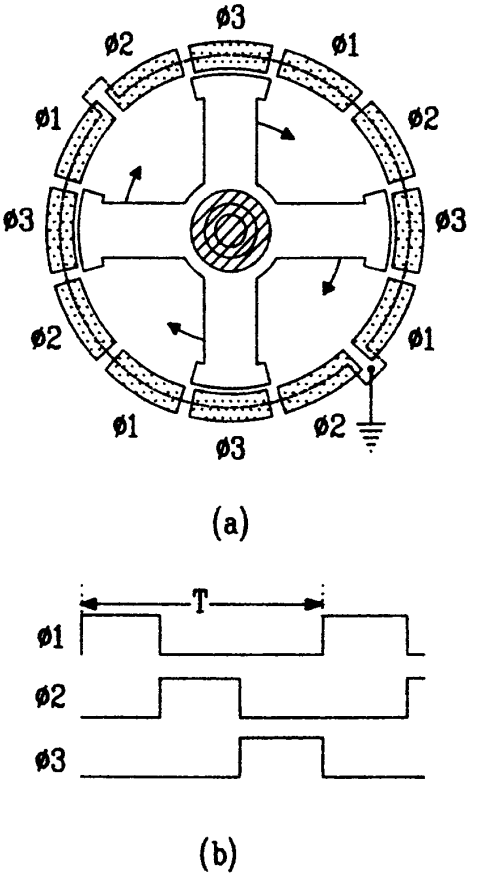

Figure 6. Electrical connections for 3-phase operation of the motor.

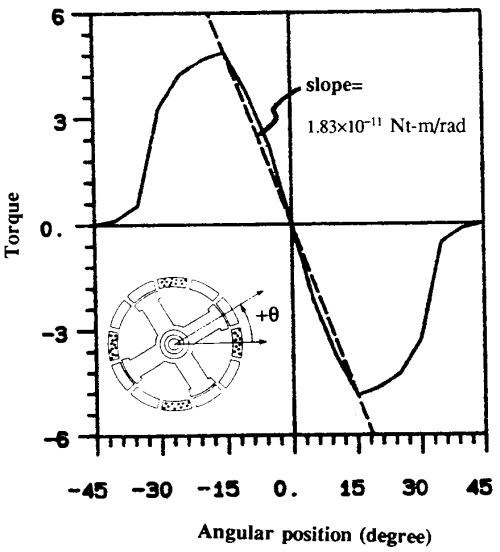

Figure 7. Torque/position characteristics of the micro-motor as obtained from two-dimensional simulation.

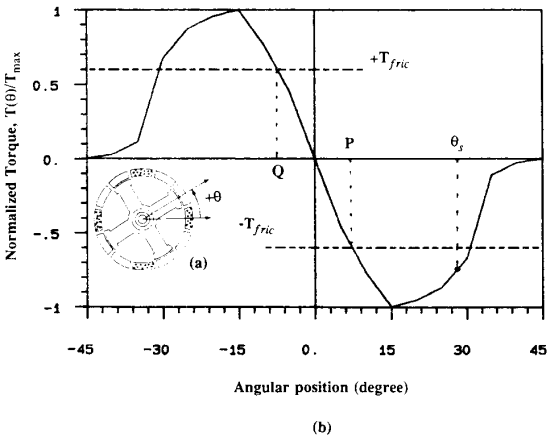

Figure 8. Single phase torque/position characteristics.

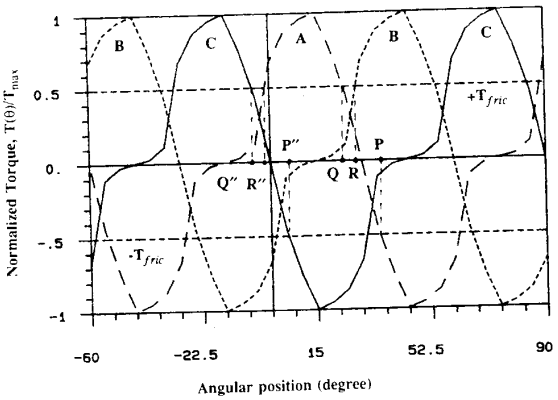

Figure 9. Three-phase torque/position characteristics.